ABSTRACT

PARKER, MATTHEW. Microfluidic Synthesis of Monodisperse Yolk-Shell Titania Microspheres as Photo-catalysts for Dry Reforming of Methane. (Under the direction of Dr. Milad Abolhasani).

Humanity is facing a climate change problem due to the increased concentration of methane and carbon dioxide in the atmosphere caused by the production, burning and transport of fossil fuels. One way to utilize these gases is through dry reforming of methane (DRM), an energy-intensive reaction that converts methane and carbon dioxide into a mixture of carbon monoxide and hydrogen gas, also called synthesis gas. A continuous photo-thermal dry-reforming strategy (*i.e.*, transparent millifluidic reactor) using a novel photocatalyst can be envisioned to reduce significantly the energy penalty associated with DRM. To achieve such a vision, a highly porous support structure (e.g., titania) for insertion of the metal catalyst is desired. In this work, a microfluidic reactor that decouples droplet formation from interfacial hydrolysis through the use of formamide as a continuous phase was used to produce titania microparticles for use as photocatalysts in the millifluidic reactor. The particles produced using this reactor have a unique yolk-shell morphology and surface areas that are ~2.5 times higher than the industry standard. Further work will be done to optimize the surface properties of these particles through tuning the composition of the dispersed phase, changing the method of UV curing and varying the ramp rates and temperature of calcination.

Microfluidic Synthesis of Monodisperse Yolk-Shell Titania Microspheres as Photo-catalysts for Dry Reforming of Methane

by
Matthew Parker

A thesis submitted to the Graduate Faculty of
North Carolina State University
in partial fulfillment of the
requirements for the degree of
Master of Science

Chemical Engineering

Raleigh, North Carolina

2019

APPROVED BY:

Dr. Milad Abolhasani Chair of Advisory Committee	Dr. Fanxing Li
Dr. Phillip R. Westmoreland	

DEDICATION

To my friends and family and everyone who has helped me through my entire educational experience.

BIOGRAPHY

Matthew Parker was born and raised in Salt Lake City, Utah. During his time in Salt Lake City, he attended West High School, where he completed the International Baccalaureate program and was a semifinalist for the National Merit Scholarship. Upon graduating from West High School in 2014, Matthew attended Barrett, The Honors College at Arizona State University in Tempe, Arizona to obtain his Bachelor's Degree in chemical engineering. While at Arizona State University, he worked on protein expression under Dr. Brent Nannenga. He graduated from Arizona State in 2017 after completing his honors thesis on Enhancing Expression Levels of Antigen-binding Antibody Fragments in *Escherichia Coli* (*E. Coli*). In the summers of 2016 and 2017, Matthew worked on a microfluidic technique known as Drop-Seq under Dr. John Phillips and Dr. Laurie Jackson at the University of Utah School of Medicine. Upon graduation from Arizona State, Matthew elected to attend North Carolina State University in order to obtain his Master's Degree in chemical engineering.

ACKNOWLEDGEMENTS

I would like to acknowledge my advisor Dr. Milad Abolhasani, who has been an invaluable help in completing this project. In addition I would like to acknowledge my other committee members Dr. Fanxing Li and Dr. Phillip Westmoreland for their guidance on this thesis.

I would also like to give a special thanks to Zachary Campbell, who has been an absolutely remarkable colleague during my time here at North Carolina State. I can say with 100% confidence that this project would not have been completed without him. In addition I would like to thank Jeffrey Bennett, Jacob Lustik and Amur Al-Rashdi. I can't thank them enough for all of their help in the completion of this thesis.

Furthermore, I would like to show my gratitude those who helped me in my research journey before my arrival at North Carolina State University. The main people I would like to thank are Dr. Brent Nannenga, Jeremy Adams, Dr. John Phillips, Dr. Laurie Jackson. The former two were my research advisor and lab partner respectively at Arizona State University, while the latter two oversaw my research at the University of Utah.

Of course I wouldn't have been able to succeed in this program without the help of my professors as well as the administrative staff here. So I would like to acknowledge Dr. Peter Fedkiw, Dr. Saad Khan, Dr. Gregory Parsons, Dr. Keith Gubbins, Dr. Albert Keung, Dr. Adriana San-Miguel, Dr. Henry Lamb, Sandra Bailey and Joan O'Sullivan.

Last, but certainly not least, I would like to thank my family and friends for their continued support through my education.

TABLE OF CONTENTS

LIST OF TABLES

LIST OF FIGURES

PREFACE

Parts of this work were previously published as part of the American Chemical Society Chemistry of Materials article *Continuous Synthesis of Monodisperse Yolk–Shell Titania Microspheres*[1] *(*Campbell, Z. S.; Parker, M.; Bennett, J. A.; Yusuf, S.; Al-Rashdi, A. K.; Lustik, J.; Li, F.; Abolhasani, M. Chemistry of Materials 2018, 30 (24), 8948–8958), which I am the second author on.

CHAPTER 1: INTRODUCTION

1.1: Climate Change Problem

Currently humanity is facing a climate change problem. Temperatures are increasing worldwide and extreme weather events are happening more frequently[2]. This climate change is primarily caused by the increasing emission of greenhouse gases, namely carbon dioxide (CO_2) and methane (CH_4). Carbon dioxide is primarily produced by combustion of fossil fuels like coal and natural gas, while methane is predominantly produced from livestock as well as the transport and production of fossil fuels[3].

The emission of these gases contributes to the "greenhouse effect", which traps heat from solar energy in the atmosphere, allowing the Earth to stay warm. However because humanity is emitting ever increasing quantities of these so-called "greenhouse gases", more heat remains trapped by the atmosphere, which is the primary cause of global warming[4].

1.2: A Possible Solution

A possible solution would be limiting the emission of greenhouse gases to the atmosphere. One way this might be achieved is by converting emitted methane and carbon dioxide to synthesis gas *via* reaction shown below, known as dry reforming of methane (DRM).[5]

$$CH_4 + CO_2 \rightarrow 2\,CO + 2\,H_2,\ \Delta H°_{298} = 247.3\ kJ/mol$$

This reaction is viewed as an attractive method of climate change mitigation for two reasons. The primary reason is that the carbon monoxide and hydrogen gas formed through this reaction can be used to form synthesis gas (syngas), which can be used as a feedstock in many industrial applications. In addition, the products can be used as reactants in the Fischer-Tropsch synthesis of higher-order hydrocarbons[6]. The use of the

products for Fischer-Tropsch reactions is particularly enticing as other methods of producing higher order hydrocarbons such as fluid catalytic cracking (FCC) produce by-products that are harmful to the atmosphere.

However as shown, this reaction is very endothermic, possessing a very high activation energy. These parameters need to be addressed in order to make DRM a viable approach to mitigate climate change.

1.3: A Photocatalytic Approach

One proposed method to get around the relatively high-energy requirement of DRM involves the use of the readily available solar energy in combination with a highly effective photocatalyst. A glass millifluidic reactor encased in a stainless steel block can be envisioned to achieve such a goal. Figure 1.1 below shows a diagram of this reactor.

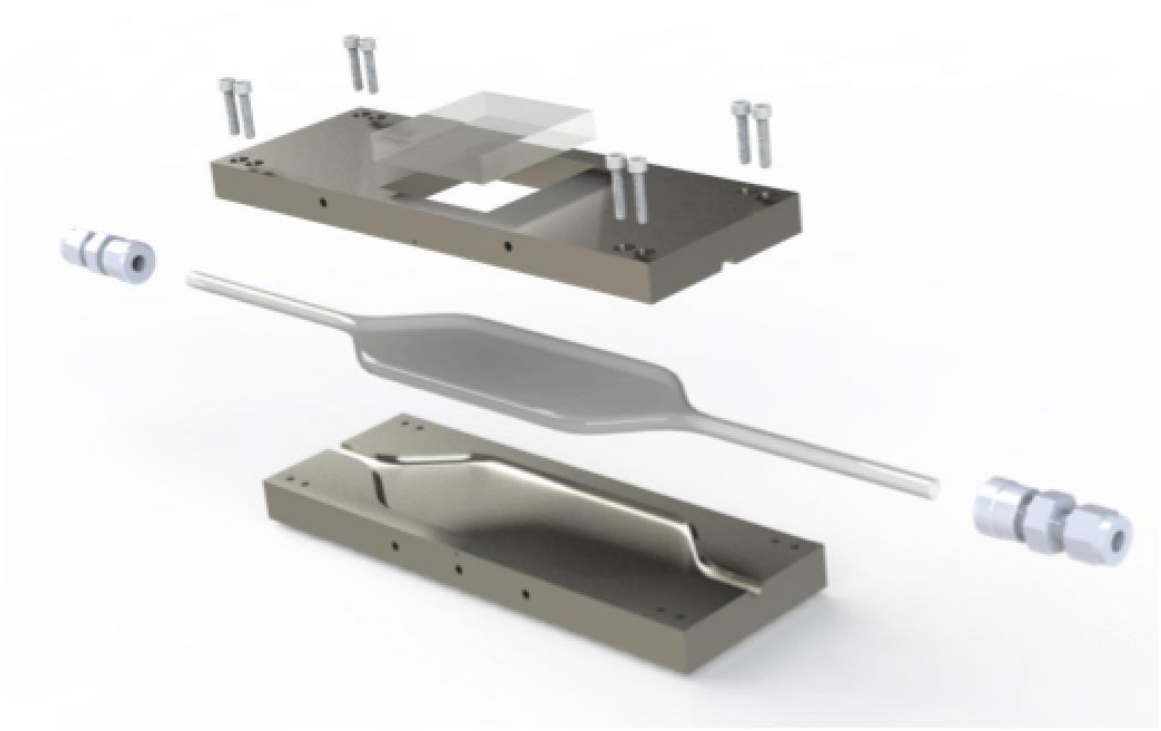

Figure 1.1: Diagram of proposed millifluidic reactor for DRM.

The reactor shown in Figure 1.1 would address the energy requirements for DRM through photo-catalysis. This reactor would be packed with a photo-catalyst that is exposed to solar light (providing energy in the form of heat and photons) through a quartz window in the top of the reactor using a solar simulator. Activated photo-catalysts can significantly decrease the energy requirement for the reaction. Photo-catalysts are typically transition metal oxides[7] such as alumina (Al_2O_3), zirconia (ZrO_2) and titania (TiO_2). This thesis will explore the use of titania as a photo-catalyst for DRM.

1.4: Why Titania?

Titania is already used in a number of fields, ranging from photovoltaics to electrochemistry due to its unique optical and physiochemical properties. One particular property about titania that is exciting for the purposes of this thesis is its relatively small band gap (3.0-3.2 eV).[8] This small band gap allows it to absorb light more easily in the visible spectrum upon being reduced (other transition metal oxides have larger bandgaps, meaning they need to undergo more treatment in order to absorb light in the visible spectrum). This property makes it an ideal material for dye-sensitized solar cells and as a photocatalyst. Titania is also a good choice as a photocatalyst due to its resistance to photo-corrosion and nontoxicity.[9]

It should be noted that titania has multiple phases with different properties. The two primary phases that occur in nature that are used for photocatalysis are known as anatase and rutile. Anatase is widely considered to be the superior photocatalyst[10,11] due to its increased bulk catalysis (the catalytic activity continues further into the surface of anatase titania than rutile titania). Anatase is known to undergo a phase transition to

rutile at or above 600ºC. This limits the temperature that reactor can be heated to, as a phase transition to rutile would decrease the photocatalytic efficiency of the system.

An ideal photo-catalyst in the proposed millifluidic reactor would cause a relatively low pressure drop in the system and have a high surface area (over 100 m^2/g). A high surface area is important as the number of active sites available for catalysis increases with surface area. Based on these two conditions, the most reasonable type of photo-catalyst would be monodisperse microparticles with a large diameter (~50 μm) hollow shell, and high porosity. The particles' monodispersity and size helps minimize the pressure drop across the reactor, while their porosity increases the surface area to the desired levels, allowing for the addition of noble metal nanoparticles. Noble metals are effective catalysts on their own, and the addition of such nanoparticles will increase the total catalytic activity of the particles. Continuous, high-throughput production of these particles is also desired as large quantities are necessary to pack the millifluidic reactor. Due to a combination of these three factors, it has been decided that microfluidics is the best method to produce these particles.

1.5: Why Microfluidics?

Microfluidics is the preferred method for synthesizing monodisperse titania microparticles due to inherent tunability and the wide parameter space that may be explored using microfluidic techniques, including the flow-rates, capillary diameter and composition of precursor. Other methods such as batch production, bulk emulsion, deposition[12] and the solvothermal method[13] do not control the size of the particles to the desired magnitude (particles produced using the solvothermal method have a diameter of ~2μm), and the particles produced through these methods have higher polydispersities

than the ones necessary for the millifluidic reactor. Through microfluidics, the size, porosity, composition, morphology and surface area of the particles can be tuned, allowing for all of these parameters to be optimized for the desired application.

Previous work on producing monodisperse titania microparticles using microfluidics has been consistent in terms of the general method of production. An oil (dispersed) phase containing a titanium precursor and a solvent is fed through an inner capillary while an immiscible continuous phase (typically water containing a surfactant breaks up the oil phase into droplets as both phases enter a constriction.[14] The titanium pre-cursor is normally titanium n-butoxide (TBT), while the solvent is typically ethoxylated trimethylolpropane triacrylate (ETPTA), 2-hydroxy-2-methyl-1-phenyl-1-propanone (HMPP), toluene or octanoic acid. The continuous phase normally contains water as well as a surfactant (Pluronic F108). These droplets are then collected in a vial containing water where the particles are permitted to fully hydrolyze, after, which they can be dried and calcined to form particles suitable for further use. A schematic of this method is illustrated below in Figure 1.2.[13]

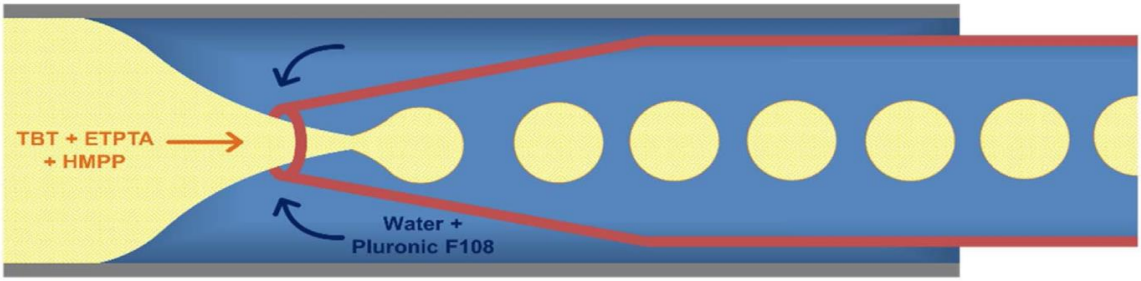

Figure 1.2: Example of microfluidic production of monodisperse titania microparticles[14].

In Figure 1.2, the yellow stream on the left labeled TBT+ETPTA+HMPP is the oil phase while the blue stream on the right is the continuous phase. Figure 2 shows how the water breaks up the oil phase by pinching the flow at the exit capillary constriction.

This method produces hollow titania microparticles *via* interfacial hydrolysis of TBT. The mechanism for this reaction is shown below in Figure 1.3.[15]

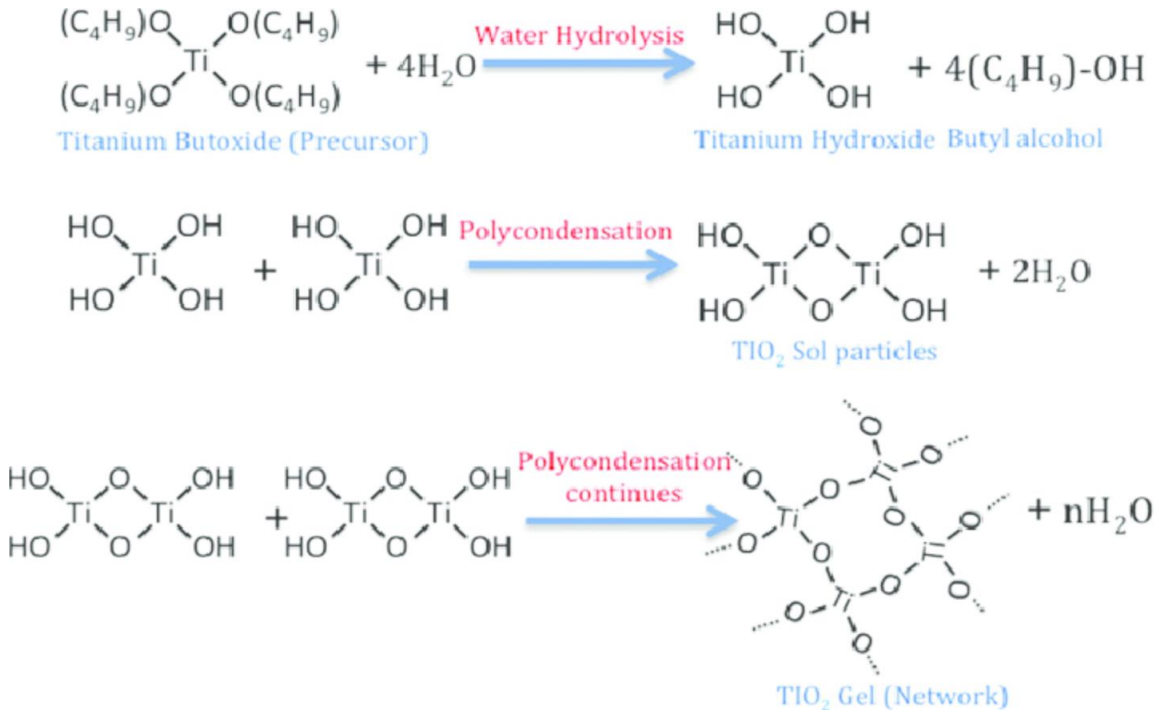

Figure 1.3: Mechanism of hydrolysis of titanium n-butoxide to form a titania network[15].

While this method does work, using water as a continuous phase can cause reactor clogging and prevent further reactor use. There are two primary methods that have been used to mitigate reactor clogging, including the use of hydrolysis-inhibiting compounds such as carboxylic acids or using low TBT concentrations. While both methods do succeed in limiting hydrolysis that occurs in the reactor, they limit the throughput (mixing TBT with octanoic acid forms a highly viscous mixture that cannot be pushed through at flowrates higher than 10 µL/minute without significantly lowering the monodispersity of the particles[11]).

1.6: Novel Approach

Our new approach instead uses formamide, a polar, aprotic solvent as the continuous phase instead of water. This prevents hydrolysis from occurring in the reactor by

decoupling droplet production from the interfacial hydrolysis that forms the titania shell. By separating the process into two discrete steps, throughput can be increased dramatically by increasing the concentration of TBT in the precursor and the total flow rate of the system can increase now that carboxylic acids can be excluded from the process in favor of toluene. This approach allows higher flow rates for synthesis of larger particles. This is an innovative method that has allowed for very high success TiO_2 microparticle production, which will be discussed in the following chapters.

CHAPTER 2: EXPERIMENTAL APPARATUS AND PROCEDURE

2.1: Design, Construction and Operation of Reactor

2.1.1: Design of Reactor

Figure 2.1 shows a diagram of the micro-reactor used for synthesizing the titania microparticles.

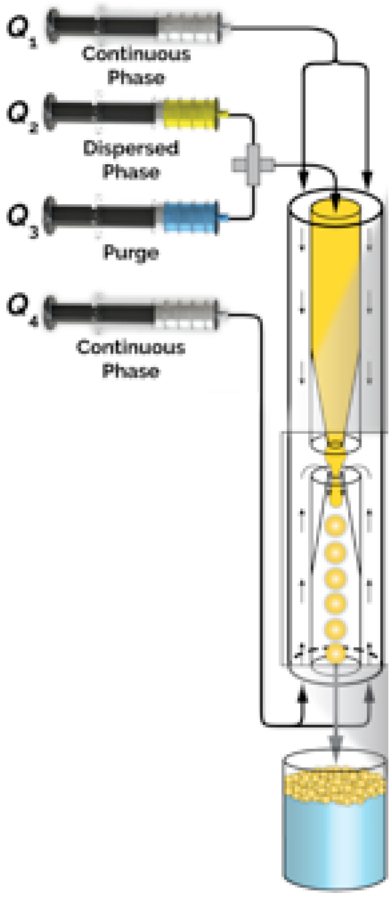

Figure 2.1: Diagram of micro-reactor used for microparticle synthesis[1].

The developed reactor produces monodisperse droplets enabled by shear forces caused by the flow of the continuous and dispersed phases through the exit capillary constriction. Two continuous-phases streams are used, at the interface between two separate internal capillaries. The continuous-phase stream that flows into the reactor

from above is known as the co-flow line, while the stream that flows into the reactor from below is known as the counter-flow line.

A purge stream was implemented to eliminate bubbles during startup and remove all precursor from the reactor to ensure the reactor's viability for future synthesis runs.

2.1.2: Chemicals and Materials

The chemicals used in the process of synthesizing the particles as well as their purposes are listed below in Table 2.1.

Table 2.1: Names and purposes of chemicals used in the synthesis process

Chemical	Purpose
Titanium tetrabutoxide (TBT)	TiO_2 precursor
Ethoxylated trimethylolpropane triacrylate (ETPTA)	Photocurable polymer in dispersed phase
Pluronic F108	Surfactant in continuous phase and collection vial
Darocur 4265	Photoinitiator in dispersed phase
Formamide	Primary component in continous phase
Toluene	Viscosity regulator in dispersed phase, primary component of purge stream
Sudan Blue II	Dye in purge stream
Deionized Water (DI Water)	Hydrolysis agent in collection vial
Isopropyl Alcohol (IPA)	Washing agent after curing

As stated in Chapter 1 and shown in Figure 2.1, there are two primary phases in the reactor: the dispersed phase and the continuous phase. The dispersed phase is made up of TBT, ETPTA, Toluene and Darocur 4265, while the continuous phase is made up of formamide and Pluronic F108. Before and after operation, the reactor is purged with a mixture of toluene and Sudan Blue II to remove bubbles or any remaining precursor. After the particles are formed in the reactor, they are collected in a vial containing DI Water and 2 wt % Pluronic F108.

Table 2.2 below lists the components used in the construction of the reactor and their purposes. From this point on, the outer diameter of an object will be referred to as the OD, while the inner diameter will be referred to as the ID.

Table 2.2: Names and purposes of components used for constructing the reactor

Component	Purpose
Glass capillary (OD of 1.5 mm, ID of 1.12 mm, initial length of 100 mm)	External capillary
Glass capillary (OD of 1.0 mm, ID of .75 mm, initial length of 100 mm)	Internal capillary
Polyether ether ketone (PEEK) T-junction (ID of .05 mm)	Connection between two unique streams
Tygon tubing (OD of 1/8'', ID of 1/16'')	Connection between external capillary and T-junction
1/8'' nuts and ferrules	Secure connection between Tygon tubing and external capillary or T-junction
1/16'' nuts and ferrules	Secure placements of internal capillaries with respect to external capillaries
4-way valve	Regulator and outlet of dispersed phase and purge stream
Fluorinated ethylene propylene (FEP) tubing (ID of 0.04'')	Connection between upper capillary and 4-way valve
FEP tubing (ID of 0.02'')	Connection between continuous phases and T-junctions

The capillaries (two internal and one external) are the primary components of the reactor, while the other components assist in regulating and securing the flow of the different input streams to the reactor.

2.1.3: Technology

The instruments used during the initial synthesis of the particles and their purposes are listed below in Table 2.3.

Table 2.3: Names and purposes of technological instruments used in the synthetic process

Instrument	Purpose
Capillary puller	Capillary modifying device used to shrink the diameter of the internal capillaries.
Gas tight syringes (1-50 ml)	Initial containment vessels for continuous and dispersed phases
Syringe pumps	Flow regulatory instrument from syringes to reactor
Microscope	Observation instrument to consistently monitor reactor activity and performance
Camera	Recording instrument to consistently monitor reactor activity and performance
Light	Illuminating instrument to consistently monitor reactor activity and performance
Mirror	Reflecting instrument to consistently monitor reactor activity and performance
Table	Self-stabilizing surface to regulate reactor conditions as much as possible
UV Lamp	Curing instrument to initiate ETPTA cross-linking after sufficient hydrolysis
Oven	Heating instrument to dry particles after washing
Muffle Furnace	Heating instrument to calcine particles after drying

2.1.4: Preparation of Mixtures Used For Reactor Operation

To prepare the dispersed phase, ETPTA and anhydrous toluene are first combined such that the mixture is 30% ETPTA and 70% toluene by weight. 100 µl of Darocur 4265 is added to this initial mixture. This mixture is then sealed in an airtight vessel and purged with nitrogen so that no air remains in the container. A disposable syringe is then used to add TBT to this initial solvent mixture until the desired concentration (from 1-30 wt%) is reached. This final phase was then mixed thoroughly so that the mixture was homogenous.

To prepare the continuous phase, Pluronic F108 was added to a container with anhydrous formamide such that Pluronic F108 made up 1% by weight of the total

mixture. Activated molecular sieves were added, and the container was sealed. The cap was fitted with 0.04'' ID FEP lines for withdrawal and venting. After sealing the container, the mixture was purged with nitrogen using the FEP withdrawal lines. The mixture was then degassed using a sonicator to minimize exposure to water.

To prepare the purge mixture, 30 mg of Sudan Blue II dye are added to 40 mL of toluene. This mixture is then homogenized.

2.1.5: Construction of Reactor

The external capillary is first cut to a length of 80 mm. The two internal capillaries were prepared by constricting one end by heating with a capillary puller. After the internal capillaries were modified, the upper internal capillary was cut to 50 mm. 1/8'' nuts and ferrules were then used in conjunction with Tygon tubing to attach the ends of the external capillary to the PEEK T-junctions. Afterwards, the modified end of upper internal capillary is inserted into one end of the external capillary, while 0.04'' FEP tubing is fitted onto the other end of the upper internal capillary, and the tube's other end is attached to the 4-way valve. Afterwards, the modified end of the lower internal capillary is positioned inside the other end of the external capillary so that the tips of the two internal capillaries are co-axial with each other and ~.7 mm apart. This position is then secured with a 1/16'' nut and ferrule. Once the position of all three capillaries are secured, 0.02'' FEP tubing is used to connect the dispersed phase and purge line syringes to the 4-way valve. Next, 0.02'' FEP tubing is used to connect the continuous phase syringes to the perpendicular ports of both T-junctions. The reactor is set up in a vertical manner so that the lower internal capillary can feed directly into the hydrolysis agent present in the collection vial.

2.2: Particle Synthesis Procedure

2.2.1: Production of Droplets

Once the syringes containing the dispersed phase, continuous phase and continuous counterflow phase are prepared, they are attached to their respective tubing lines and placed in syringe pumps. The syringe pumps are then programmed with the desired flow rate for the experiment. The flow rate for the dispersed phase stream is kept between 10 and 50 μL/minute, while the flow rate for the continuous phase streams is kept between 50 and 150 μL/minute. The two continuous-phase streams use the same flow rates and are therefore operated by the same syringe pump.

2.2.2: Curing

After collection, the droplets are allowed to hydrolyze for 1.5 hours. Following hydrolysis, a 365 nm UV lamp is shined on the particles for 10 minutes, during which the vial is periodically swirled so all microparticles are fully cured. This curing step stops hydrolysis by crosslinking the ETPTA in the particles, forming a solid network. In addition, this step causes the formation of two distinct regions in each microparticle: a core comprised of unreacted TBT, crosslinked ETPTA, and toluene, and a shell consisting of titania, ETPTA and toluene.

2.2.3: Washing and Drying

After crosslinking, the microparticles are filtered out and washed with water. The microparticles are rinsed 3-4 times to ensure that all formamide and Pluronic F108 are removed to minimize the chances of any undesirable compounds forming during the calcination step. The microparticles are then dried overnight in an oven at 90º C. During

the drying step, the diameter of the particles decreases substantially as toluene is removed from the surface of the particle.

2.2.4: Calcination

Once the particles have been thoroughly washed and dried, they are placed in an alumina crucible and calcined in a muffle furnace 500º C for 1 hour (5º C/minute).

A schematic of the post-collection procedure and the effects of each step on the particle is shown below in Figure 2.2.

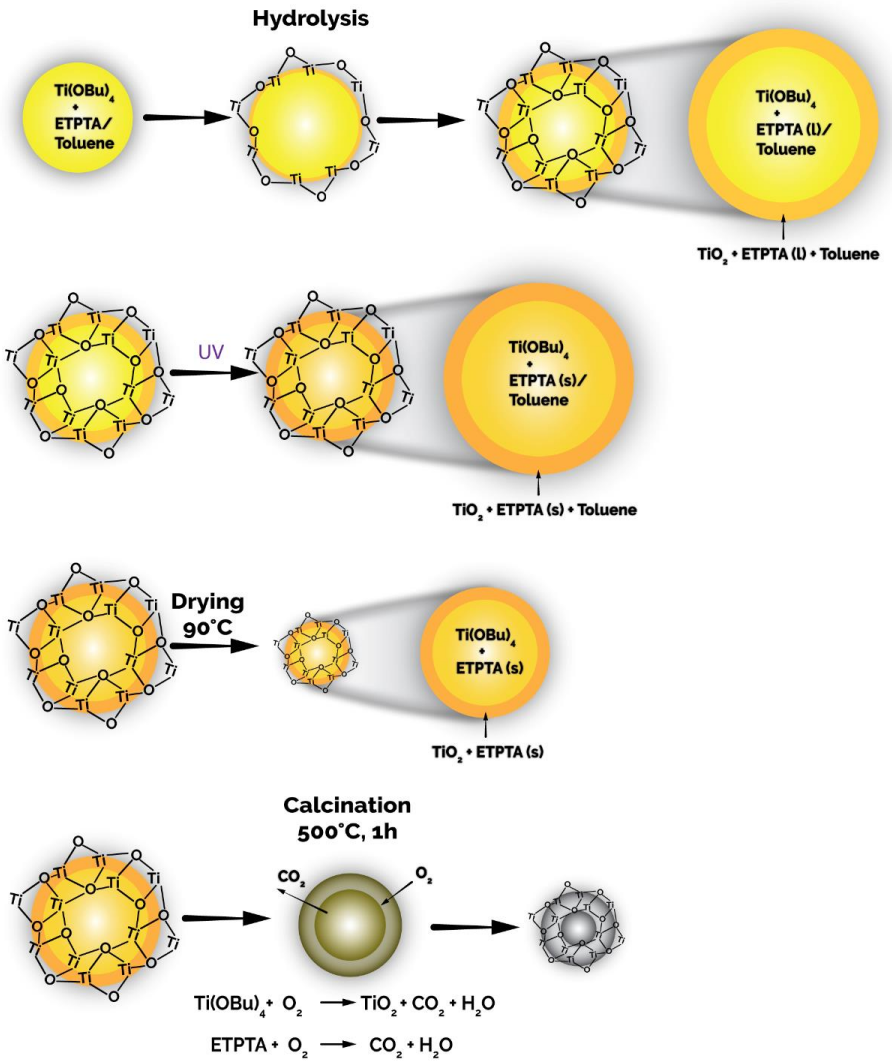

Figure 2.2: Schematic of post-collection steps of production of titania microparticles and their impact on the present chemical composition[1].

CHAPTER 3: PARTICLE CHARACTERIZATION AND ANALYSIS

3.1: Imaging and Characterization Methods

In order to catalogue the attributes of the particles at all steps of the synthesis process, various imaging and characterization techniques were used. All characterization techniques are outlined in Table 3.1.

Table 3.1: Names and purposes of imaging and characterization technologies used to analyze the particles

Imaging/Characterization Technology	Measurements Performed
MATLAB	Diameter of in-situ, collected, dried particles, frequency of particle production.
ImageJ	Diameter, polydispersity of calcined particles
Brunauer-Emmett-Teller (BET)	Specific surface area, porosity of calcined particles.
Scanning Electron Microscopy (SEM)	Diameter, shell thickness of dried, calcined particles.
X-Ray Diffraction (XRD)	Phase composition of calcined particles (performed in-situ).

The methods listed above were used to obtain a thorough analysis of the particles produced using the procedure detailed in Chapter 2. The rest of this chapter will show the images and measurements obtained using these methods and how they can be compared to similar measurements of other particles.

3.2: Particle Diameter Analysis

The first parameter analyzed to ensure the quality of the microparticles was the monodispersity, which is desired to ensure minimal pressure drop in the reactor. The coefficient of variation (CV), a commonly used metric to determine particle monodispersity, is calculated using the following formula: $CV=\sigma_D/<D>\times100$,where CV is the coefficient of variation, σ_D is the standard deviation of particle diameter, and $<D>$ is the average particle diameter. Microparticle size distribution was analyzed at three

different stages of the production process: after collection, after drying and after calcination. For the first two stages, the diameter and CV were measured using a custom MATLAB image processing code (Appendix A). A sample image output can be found in Appendix B. For the third stage, the diameter and CV were measured using ImageJ.

Five sets of flow rates were used to analyze size variation and microparticle shrinkage across different flow rates (shown in Table 3.2). For these flow rate studies, the TBT concentration was kept constant at 5 wt%.

Table 3.2: Flow Rate sets used for size analysis

Flow Rate Set	Dispersed Phase Flow Rate (µL/min)	Continuous Phase Co-Flow Flow Rate (µL/min)	Continuous Phase Counter-Flow Flow Rate (µL/min)
1	30	50	50
2	30	75	75
3	30	100	100
4	30	125	125
5	30	150	150

Figure 3.1 below shows the images used to find the diameter and polydispersity as well as the resulting histograms for particles that were produced using the flow rates described in Flow Rate Set 5 in Table 3.2.

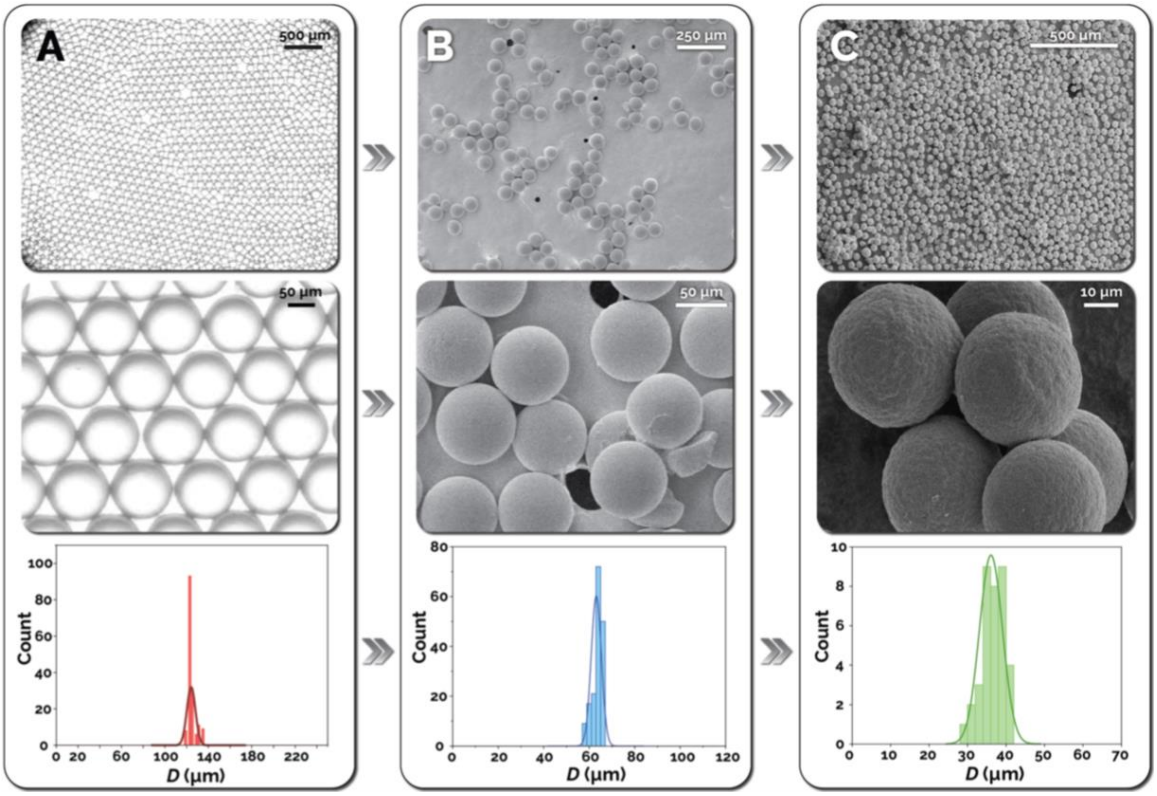

Figure 3.1: Pictures and resulting histograms of particles produced at the flow rates for Flow Rate Set 1[1].

In Figure 3.1, Column A shows particles post-collection, Column B shows particles post-drying, and Column C shows particles post-calcination. The histograms at the bottom of the columns show that there is very low polydispersity (<3% CV in the post-collection column), meaning that these particles are sufficiently monodisperse during all steps of the production process. Particles synthesized with other flow rates exhibited similar CV values.

Figure 3.2 below shows the average diameters of the particles at all three stages of the process for all five flow rate sets. The red bars represent the average diameter of the particles immediately after collection, blue bars represent the average diameter of the particles after they have been dried, and green bars represent the average diameter of the particles after they have been calcined.

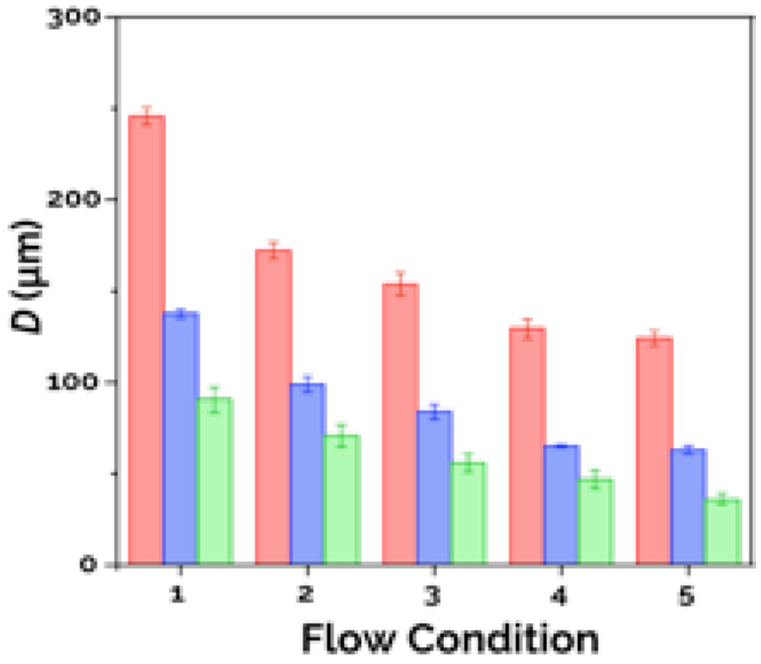

Figure 3.2: Average diameter of particles produced using different flow sets during different stages of production[1].

Figure 3.2 demonstrates the impact of flow rates on particle diameter. As the ratio of dispersed phase to continuous phase (Q_D/Q_c) decreases, the particles become consistently smaller. Figure 3.2 also shows that the decrease in particle diameter after drying and calcination stays consistent across different flow rate sets, as drying had a larger effect on the particle diameter than calcination. The decrease in particle diameter after drying was found to range from 42-50%, while the decrease in particle diameter after calcination was found to range from 28-43%.

The results show that the sizes of the particles produced using this method are an order of magnitude larger than those produced with solvothermal and deposition/etching methods. This is favorable; as the larger particles will cause a lower pressure drop in the reactor compared to the smaller particles produced using other methods.

3.3: Surface Area Analysis

The second parameter analyzed to assess the microparticles was surface area. High surface area is desirable for heterogeneous catalysis because the quantity of active sites increases with surface area. The surface area was analyzed using BET (N_2). Figure 3.3 shows the measured specific surface areas of calcined particles produced using different concentrations of TBT.

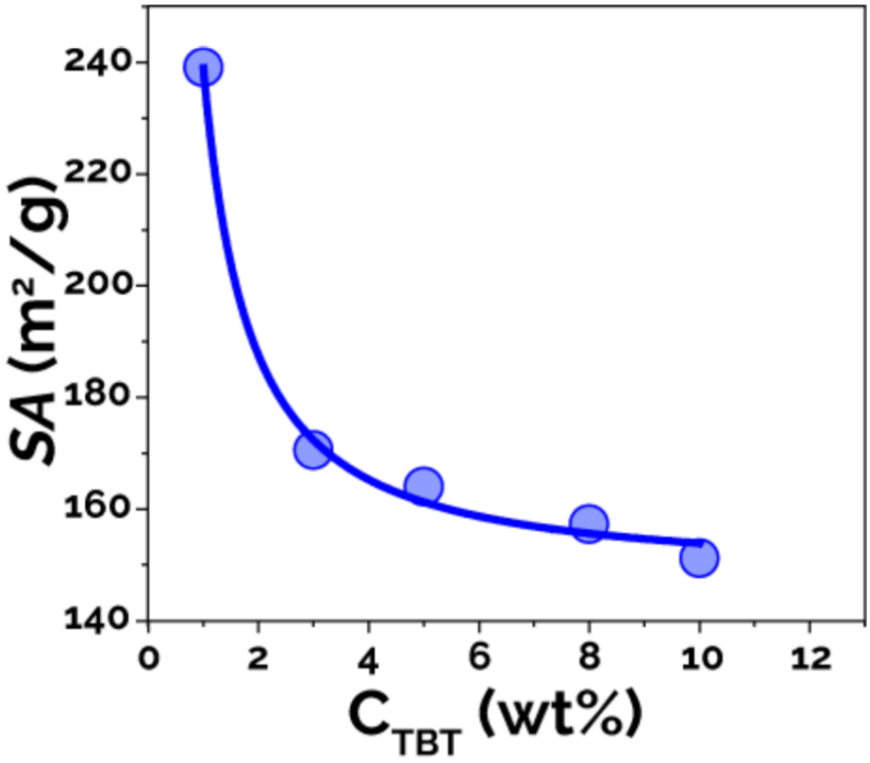

Figure 3.3: Surface area measurements made on titania microparticles produced using different concentrations of TBT[1].

Figure 3.3 shows that the surface areas measured using BET ranged from 151 m^2/g at 10 wt% TBT to 239 m^2/g at 1 wt% TBT. For comparison, the commercial standard for titania particles (Degussa P25) has a surface area of ~65-75 m^2/g.[16] This proves that the reactor is capable of producing particles with high surface areas even at higher concentrations of TBT in the dispersed phase.

In addition, Figure 3.3 demonstrates that surface area decreases as TBT concentration increases. This decrease is likely caused by the increased titania density resulting in fewer/smaller pores, thus lowering the total pore volume and corresponding surface area.

3.4: Phase Composition Analysis

The third parameter analyzed to assess the microparticles was the phase composition of the titania. Ideally, the particles would consist of primarily anatase phase to maximize the photocatalytic activity of the particles. In order to test the phase composition of the titania of the particle, in-situ XRD was performed on particles produced using varying concentrations of TBT in the dispersed phase. Figure 3.4 below shows the results obtained this method with reference anatase and rutile spectra on the bottom and top of the chart, respectively.

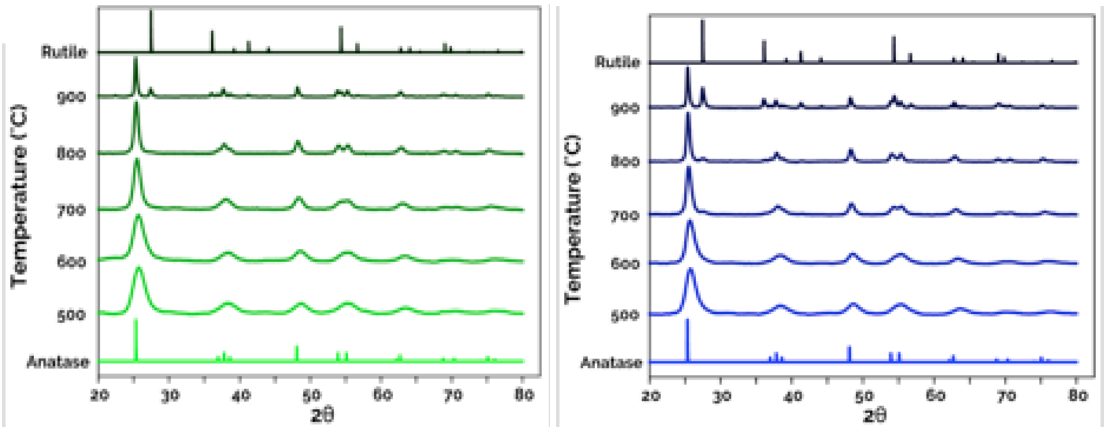

Figure 3.4: XRD Spectra from particles produced using 1 (green) and 10 (blue) wt% TBT in dispersed phase with reference anatase and rutile phase spectra[1].

Figure 3.4 shows that the rutile phase is more prominent in microparticles that were produced with a higher concentration of TBT in the dispersed phase. At 900ºC (above the transition temperature), the microparticles produced using 1 wt % TBT were

still almost entirely in the anatase phase, while the rutile phase was much more prevalent in microparticles produced using 10 wt % TBT.

Further tests were performed on particles produced using 10 wt % TBT in the dispersed phase. These tests used relative intensity ratio (RIR) analysis to find the exact phase composition of particles produced using 10 wt% TBT in the dispersed phase. These results can be found in Figure 3.5. In Figure 3.5, orange bars correspond to the anatase phase, while green bars correspond to the rutile phase.

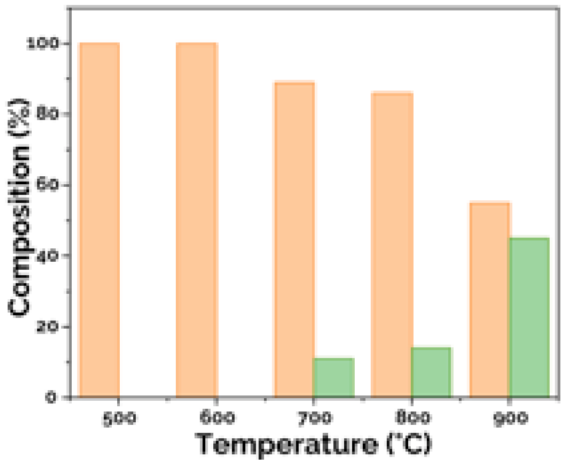

Figure 3.5: Phase composition of particles produced using 10 wt % TBT in the dispersed phase[1].

Figure 3.5 shows that at temperatures up to 600º C, there is no measurable phase transition. Between 600 and 800º C, phase transition slowly starts occurring, as there are small amounts of visible rutile phase at 700 and 800º C. Between 800 and 900º C, the phase transition appears to accelerate rapidly, as the amount of rutile phase present at 900º C is over double the amount present at 800º C.

3.5: Morphology Analysis

The final quality of the microparticles that was analyzed was the morphology. This was done using SEM after the particles were calcined. Figure 3.6 shows SEM images of microparticles produced using various concentrations of TBT in the dispersed phase.

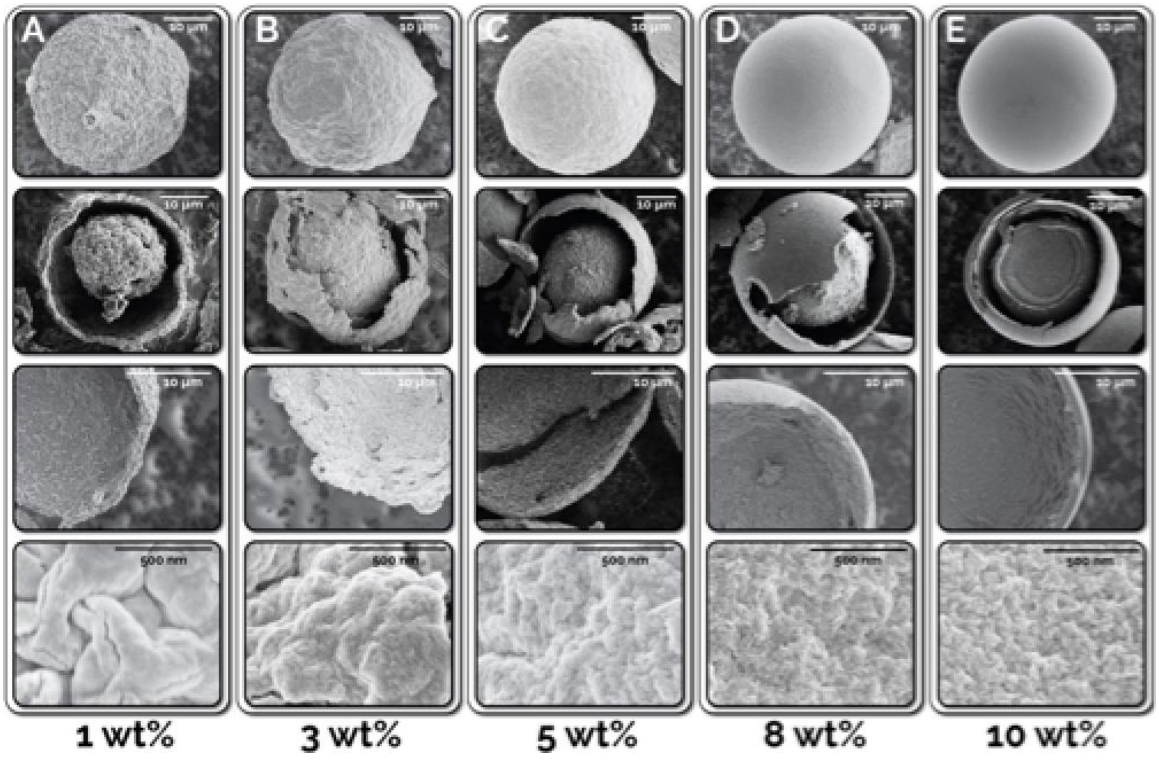

Figure 3.6: SEM images of calcined particles produced using different concentrations of TBT in the dispersed phase[1].

Figure 3.6 reveals that these particles possess an interesting yolk-shell morphology after calcination. This is due to the fact that the hydrolysis of TBT is stopped after 1.5 hours through UV curing of the particles. As mentioned previously in Chapter 2, after UV curing, the particle has two sections: the outer shell, which contains primarily titania, and the inner core, which contains TBT, though it also contains solid ETPTA (as well as toluene, which is removed during the drying step. The TBT remains in the center of the particle until the calcination step, when it oxidizes to form titania. Calcination also causes the ETPTA remaining in the core to combust, and it is this

additional process that allows for the formation of the yolk-shell morphology visible in Figure 3.6.

Figure 3.6 also demonstrates how surface morphology is affected by dispersed phase TBT concentration. When production is performed with lower concentrations of TBT in the dispersed phase, the surface of the resulting particles is quite rough and has lower density, while the opposite is true when production is performed with higher concentrations of TBT in the dispersed phase. The SEM images shown in Figure 3.6 also further explain the results given in Figure 3.3. The lower nanocrystal density observed in microparticles synthesized with lower TBT concentrations results in higher specific surface areas. The relative smoothness of the particles made with high TBT concentrations is a result of greater titania nanocrystal density, which results in lower specific surface areas.

CHAPTER 4: CONCLUSION

4.1: Assessment of Particles

The microparticles are of a relatively large size (on the order of 100 microns in diameter), have a high surface area (between 150 and 240 m^2/g), have a favorable morphology (yolk-shell) and possess the desirable phase composition at the temperatures that will be reached in the millifluidic reactor (>80% anatase). In addition, these particles display remarkable monodispersity. When taking all of these factors into account, it appears that these particles are superior to any other available titania photo-catalyst for use in the millifluidic reactor.

The particles produced using the microreactor are unique in terms of their overall attributes. While other methods have produced microparticles with higher surface areas, the microparticles produced using our microfluidic method are an order of magnitude larger, which makes them more ideal for use in the millifluidic reactor.

4.2: Overall Improvement On Previous Work

The method demonstrated improves on previous synthetic methods in a number of ways. Through the decoupling of droplet production from hydrolysis, a much higher rate of production can be reached. Through this process, production of calcined particles can reach 100 mg/hour in a single-channel reactor. Furthermore, the decoupling improves the lifetime of the used microreactor as the risk of clogging due to rapid in-reactor hydrolysis is greatly reduced. In addition, particles produced using this method have proved to have exceptional tunability, as the surface area, particle diameter, phase composition, and surface density can all be changed with relative ease.

4.3: Future Work

The unique surface morphology of the particles can be studied further. One way to do so would be to collect the particles in a dry solvent, preventing hydrolysis altogether and producing solid particles that would have similar properties to the core of the yolk-shell particles. A different method to study the morphology would be to allow the droplets hydrolyze for extended periods of time, creating particles with attributes that are like those of the shell of the yolk-shell properties. We have started experimenting with the use of a collimated UV light for the purpose of curing the droplets *in-situ*. This method is only viable for synthesizing microparticles that do not undergo any hydrolysis.

In addition, the concentration of TBT in the dispersed phase could be increased. Due to the decoupling of the droplet production from hydrolysis, there are no risks of clogging the reactor due to higher TBT concentrations. In theory, the TBT concentration could be raised significantly, which would further solidify the particles and increase density.

Lastly, the ramp rates of the calcination process can be modified. During the experiments, the ramp rate was kept constant at 5ºC/minute. Changing the ramp rates could modify the surface properties of the particles. If the modifications to the surface properties are significant enough, they could be used to further optimize the catalytic performance of the particles.

REFERENCES

1. Campbell, Z. S.; Parker, M.; Bennett, J. A.; Yusuf, S.; Al-Rashdi, A. K.; Lustik, J.; Li, F.; Abolhasani, M. Chemistry of Materials 2018, 30 (24), 8948–8958.
2. UCI study finds dramatic increase in concurrent droughts, heat waves https://news.uci.edu/2015/08/31/uci-study-finds-dramatic-increase-in-concurrent-droughts-heat-waves/.
3. Sources of Greenhouse Gas Emissions https://www.epa.gov/ghgemissions/sources-greenhouse-gas-emissions.
4. Climate change causes: A blanket around the Earth https://climate.nasa.gov/causes/.
5. Arora, S.; Prasad, R. RSC Advances 2016, 6 (110), 108668–108688.
6. Mahmoudi, H.; Mahmoudi, M.; Doustdar, O.; Jahangiri, H.; Tsolakis, A.; Gu, S.; Lechwyszynski, M. Biofuels Engineering 2017, 2 (1), 11–31.
7. Batzill, M. Energy & Environmental Science 2011, 4 (9), 3275.
8. Kavan, L. Electrochemistry and dye-sensitized solar cells. *Curr. Opin. Electrochem.* **2017**, *2*, 88-96.
9. Titania - photocatalyst for waste water decontamination http://www.mvt.ovgu.de/mvt_media/Vorlesungen/VO_ENAP/Folien_ENAP_10.pdf
10. Luttrell, T.; Halpegamage, S.; Tao, J.; Kramer, A.; Sutter, E.; Batzill, M. Scientific Reports 2014, 4 (1).
11. Li, D. Microscopy and Microanalysis 2016, 22 (S3), 824–825.
12. Chen, L.; Yang, Y.; Jiang, D. Journal of the American Chemical Society 2010, 132 (26), 9138-9143

13. Joo, J. B.; Zhang, Q.; Lee, I.; Dahl, M.; Zaera, F.; Yin, Y. Advanced Functional Materials 2011, 22 (1), 166–174.
14. Eun, T. H.; Kim, S.-H.; Jeong, W.-J.; Jeon, S.-J.; Kim, S.-H.; Yang, S.-M. Chemistry of Materials 2009, 21 (2), 201–203.
15. Eskandarloo, H.; Zaferani, M.; Kierulf, A.; Abbaspourrad, A. Applied Catalysis B: Environmental 2018, 227, 519–529.
16. Khodaparast, P.; Ounaies, Z. Smart Materials and Structures 2014, 23 (10), 104004.

APPENDICES

APPENDIX A: MATLAB CIRCLE DETECTION CODE

```
%%
clear all
close all
clc
%%
thresh=input('Input Circularity Threshold:'); %circularity threshold
%thresh= 0.8;

%%Message Strings
msgstr1 = 'Pre-Curing';
msgstr2 = 'Post-Curing';

%Prompt User for File Input and record selection
for i = 1:2
    if i == 1
        waitfor(msgbox(['Select ',  msgstr1 , ' image.']));
    else
        waitfor(msgbox(['Select ',  msgstr2 , ' image.']));
    end
    [file,path] = uigetfile('.jpg');
    files(i) = string(file);
    filepath(i,:) = string(path)+string(file);
end
%%
conditions = strsplit(files(1),'-');
outpath = path + conditions(1)+'-'+conditions(2)+'-'+conditions(3)+'-
'+conditions(4)+'-'+conditions(5)+'.txt';
file=fopen(outpath,'w');
%initialize data map
circledata = containers.Map({'test'},{[]});

%initialize figures
dist = figure('name', 'Gel Size');
hist = figure('name', 'Gel Size Histogram');

%loop over supplied images
tolscale = 0;
%%
for img = 1:length(filepath)

    %Extract magnification from image filename
    conditions = strsplit(files(img),'-');
    magcel = strsplit(char(conditions(4)),'X');
    mag = str2double(strrep(char(magcel(1)),'_','.'));

    %set scale based on magnification
    if mag == .78
        scale = 0.0467; %size of each pixel (pixels/um)
    elseif mag == 1
        scale = 0.0585;
    elseif mag == 1.25
        scale = 0.075;
    elseif mag == 1.6
        scale = 0.096;
```

```
    elseif mag == 2
        scale = 0.1207;
    elseif mag == 2.5
        scale = 0.1493;
    elseif mag == 3.2
        scale = 0.196;
    elseif mag == 4
        scale = 0.244;
    elseif mag == 5
        scale = 0.304;
    elseif mag == 6.3
        scale = 0.388;
    elseif mag == 8
        scale = 0.496;
    elseif mag == 10
        scale = 0.6227;
    elseif mag == 12.5
        scale = 0.78;
    elseif mag == 16
        scale = 1.008;
    else
        error('Not a valid magnification. Use one of the following:\n
[0.78 1 1.25 1.6 2 2.5 3.2 4 5 6.3 8 10 12.5 or 16]');
    end

    scalebars = [100 250 500 1000];
    for i = 1:length(scalebars)
        bars(i) = round(scale * scalebars(i));
    end

    %initialize throwaway figure and load image for user supplied crop
mask
    crop = figure;
    a=imread(char(filepath(img)));

    %user crop
    [x,y,mask,xi,yi] = roipoly(a);
    xmax = max(round(xi));
    xmin = min(round(xi));
    ymax = max(round(yi));
    ymin = min(round(yi));

    %scaling image bounds
    a = a(ymin:ymax,xmin:xmax,:);

    %display cropped image for radius range measurments
    figure(crop);
    imshow(a)
    imdistline;

    %prompt user for radius range
    rmax = input('Upper Bound of Diameter in px:')/2;
    if mod(rmax,1)~=0
       error('Diameter must be even')
    end
    rmin = input('Lower Bound of Diameter in px:')/2;
    if mod(rmin,1)~=0
```

```
       error('Diameter must be even')
    end
    close(crop)
    r_range=[rmin rmax];   % pixel range of radius

    %convert to grayscale, apply mask, and increase contrast
    a=rgb2gray(a);
    croppeda = a;
    scalea = a;
    for i = 1:length(bars)
        scalea(:,:,i) = a;
        scalea(floor(size(scalea,1)*.9)-
floor(size(scalea,1)*.03/4):floor(size(scalea,1)*.93)+floor(size(scalea
,1)*.03/4),floor(size(scalea,2)*.07)-
floor(size(scalea,1)*.03/4):floor(size(scalea,2)*.07)+bars(i)+floor(siz
e(scalea,1)*.03/4),i) = 0;

scalea(floor(size(scalea,1)*.9):floor(size(scalea,1)*.93),floor(size(sc
alea,2)*.07):floor(size(scalea,2)*.07)+bars(i),i) = 255;
    end
    a = a.*uint8(mask(ymin:ymax,xmin:xmax));
    b=imadjust(a);

    %circular hough transform to extract circle position and radii
    [accum, circen, cirrad] = CircularHough_Grd(b, r_range,thresh);

    %If circles are at the edge of masked region remove them
    n = 1;
    for i = 1:length(circen)
        try
            if (a(round(circen(i,2)),round(circen(i,1)+cirrad(i))) ~=
0)&&(a(round(circen(i,2)),round(circen(i,1)- cirrad(i))) ~= 0)...
                    &&
(a(round(circen(i,2)+cirrad(i)),round(circen(i,1))) ~= 0)&&
(a(round(circen(i,2)-cirrad(i)),round(circen(i,1))) ~= 0)...
                    && (cirrad(i)>= .5*rmin)
                circenbound(n,:) = circen(i,:);
                cirradbound(n) = cirrad(i);
                n = n+1;
            end
        catch
            %continue
        end
    end

    %if circles are significantly smaller than the rmin and mean remove
    %them
    n = 1;
    for i = 1:length(cirradbound)
       if cirradbound(i) > .9*mean(cirradbound)
           circenthresh(n,:) = circenbound(i,:);
           cirradthresh(n) = cirradbound(i);
           n = n+1;
       end
    end
    circen = circenthresh;
    cirrad = cirradthresh';
```

```
    %Extract solvent condition
    solcel = strsplit(char(conditions(5)),'.');
    solvent = char(solcel(1));

    %apply center intensity threshold
    edgethresh = 180;

    %if circle center is dark remove it
    try
        if strcmp(solvent ,'water')
            n = 1;
            for i = 1:length(cirrad)
                if b(round(circen(i,2)),round(circen(i,1))) >
edgethresh
                    circenthresh(n,:) = circen(i,:);
                    cirradthresh(n) = cirrad(i);
                    n = n + 1;
                end
            end
        end
    catch
        %Do nothing
    end
    circen = circenthresh;
    cirrad = cirradthresh';

    %clear vars for next loop
    clear('circenthresh','cirradthresh','circenbound','cirradbound')

    %calculate average radius and volume, stdev, and polydispersity
    ciravgrad(img) = mean(cirrad)/scale;
    stdevrad(img) = std(cirrad)/scale;
    polydisp = stdevrad./ciravgrad;
    volavg = 4/3*pi*ciravgrad.^3;

    %fill data map
    str = sprintf('%i',img);
    circledata(str) = [circen,cirrad];

    %initialize figure for circle display
    f = figure('name',char(files(img)));
    passed = 0;
    for i = 1:length(scalebars)
        if ciravgrad(img) < scalebars(i)/3 && passed == 0 && img == 1
            imshow(scalea(:,:,i));
            imgscale = scalebars(i);
            tolscale = i;
            passed = 1;
        end
        if img == 2 && tolscale ~= 0
            imshow(scalea(:,:,tolscale))
            imgscale = scalebars(tolscale);
        end
    end
    if passed == 0 && tolscale == 0
        imshow(croppeda);
```

```
    end
    hold on;

    %if circle centers are very close use larger
    for i = 1 : size(circen, 1)-1
        for j=1: 1 : size(circen, 1)-1
            d=sqrt((circen(i,1)-circen(j,1))^2+(circen(i,2)-
circen(j,2))^2);

            if d<=15
                if cirrad(i)>=cirrad(j)
                    cirrad(j)=cirrad(i);
                    circen(j,1)=circen(i,1);
                    circen(j,2)=circen(i,2);
                else
                    cirrad(i)=cirrad(j);
                    circen(i,1)=circen(j,1);
                    circen(i,2)=circen(j,2);
                end
            end
        end
    end

    %plot circle centers
    plot(circen(:,1), circen(:,2), 'r+');

    %plot circle edges
    plot(circen(:,1), circen(:,2), 'r+')

    %save figure with plotted circles and scalebar
    imgstr = strsplit(files(img),'.');
    figfile = char(path + imgstr(1) + '-processed');
    saveas(f,figfile);

    %save circle data
    fprintf(file,files(img)+'\n');
    fprintf(file,'Circularity Threshold:%4.6f\n',thresh);
    fprintf(file,'Rmin:%4.6f\nRmax:%4.6f\n',rmin,rmax);
    try
        fprintf(file,'Scale bar is:%4.6f micron\n',imgscale);
    catch
        %nothing
    end
    fprintf(file,'Circle_Number Radius(Pixels) Radius(um)\n');

    for i=1:length(cirrad)
       fprintf(file,'%4.6f %4.6f %4.6f\n', i, cirrad(i),
cirrad(i)/scale);
    end


    %plot circle size vs circle #
    figure(dist);
    hold on;

%plot(cirrad/scale,'o','MarkerEdgeColor','k','MarkerFaceColor','r','Mar
kerSize',7);
```

```
    plot(cirrad/scale,'o');
    xlabel('number');
    ylabel('radius');
    %axis([0 100 min(cirrad)/scale*.9 max(cirrad)/scale*1.1]);

    %plot histogram
    figure(hist);
    hold on;
    histfit(cirrad/scale);
    xlabel('radius');
    ylabel('frequency');
    %axis([min(cirrad)/scale*.9 max(cirrad)/scale*1.1 0 100]);

end

%save distribution and histogram figures
diststr = char(path + conditions(1) + '-' + conditions(2) + '-' +
conditions(3) + '-' + conditions(4) + '-dist');
saveas(dist,diststr);
histstr = char(path + conditions(1) + '-' + conditions(2) + '-' +
conditions(3) + '-' + conditions(4) + '-hist');
saveas(hist,histstr);

%calculate swelling ratio
swelling = (volavg(1)-volavg(2))/volavg(2);
fclose(file);
```

APPENDIX B: SAMPLE OUTPUT OF MATLAB CIRCLE DETECTION CODE